SEMARAK ILMU PUBLISHING

Journal of Advanced Research in Applied Sciences and Engineering Technology

Journal homepage:
https://semarakilmu.com.my/journals/index.php/applied_sciences_eng_tech/index
ISSN: 2462-1943

Environmental Impacts on the RSS-Based Visible Light Indoor Positioning System

Foong Jun Kit[1], See Yuen Chark[1,*], Hadi Guna[1], Harry Ramza[2]

[1] Department of Electrical and Electronic Engineering, Lee Kong Chian Faculty of Engineering and Science, Universiti Tunku Abdul Rahman, 43000 Kajang, Selangor, Malaysia
[2] Universitas Muhammadiyah Prof. Dr. Hamka, Jakarta 12130, Indonesia

ARTICLE INFO

Keywords:
Indoor positioning system (IPS); Visible light; Non-line-of-sight (NLOS); Received signal strength (RSS); Trilateration

ABSTRACT

To address the shortcomings of the global positioning system (GPS) operating within indoor scenarios, a range of indoor positioning systems (IPS) have been proposed. Among these, visible light IPS garners substantial research interest for its potential as a cost-effective IPS solution. However, susceptibility to environmental influences like external light and non-line-of-sight that can significantly affect its performance hindered its adoption. Hence, a simulation framework capable of simulating these influences becomes crucial in supporting the effective deployment and promoting the adoption of visible light IPS. This paper investigates the feasibility of using a simulation framework to replicate environmental factors affecting the system, including external optical sources and blocked transmitters. The research involved the development of a received signal strength (RSS) based visible light IPS prototype and an associated simulation framework. Subsequently, the prototype was tested in three distinct environments: no influences, with an external optical source, and non-line-of-sight. The prototype achieved an accuracy of 0.0836 m, 0.3541 m, and 1.1519 m for 50% of the time respectively in these three environments. Ultimately, the simulation framework developed is capable of reproducing similar effects for all three environments with a difference in the accuracy of 76.08%, 74.86% and 867%, respectively. Thus, the findings support the use of the developed simulation framework for the effective development of visible light IPS in environments with no influences and with external optical sources.

1. Introduction

Global Navigation Satellite Systems (GNSS), such as the Global Positioning System (GPS) and the Global Navigation Satellite System (GLONASS), are unable to provide accurate and stable navigation in the indoor environment. An Indoor Navigation System (INS) is a technology that can provide precise localization and the navigation of objects or people in the indoor environment. A reliable INS is also a crucial tool for location-based services. Additionally, between 2022 and 2027, the market for INSs is predicted to increase at a compound annual growth rate of 34.07% as stated in the report [1].

* *Corresponding author.*
E-mail address: seeyc@utar.edu.my

https://doi.org/10.37934/araset.55.1.6381

INS is a system comprising three major parts: namely, the navigation module, human-machine interface and indoor positioning system (IPS) module introduced by Kunhoth *et al.,* [2]. Among these, the IPS module is an important part that estimates the position of an object or a human. To date, numerous types of technology have been proposed for IPS, each with its advantages and disadvantages. To simplify the comparison among the existing technologies proposed, we can categorise them into two categories: radio-frequency (RF)-based and non-RF-based. For instance, RF-based technologies are wireless fidelity (Wi-Fi), Bluetooth low energy (BLE), ultra-wideband (UWB), RF identification (RFID), and ZigBee. On the other hand, non-RF-based technologies are visible light and ultrasonic. The overview of the categorised IPS technologies is illustrated in Figure 1.

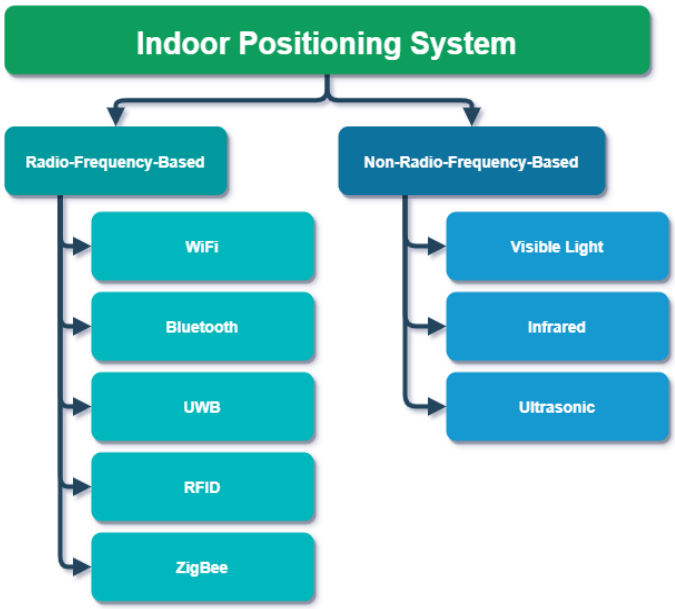

Fig. 1. Indoor Positioning System Technologies Overview

Among the technologies mentioned, visible light was opted as the technology to realize the IPS in this research. The potential of a visible light IPS (VLIPS) is not only limited to navigation and social distancing monitoring purposes. To date, there has been an increasing number of studies on the applications of the VLBS. For example, one potential application is light fidelity (Li-Fi) discussed in the previous study [3]. The VLIPS requires light-emitting diodes (LEDs), which have higher luminous efficacy than the conventional lightings [4], as signal transmitters and the photodiodes or phototransistors as signal receivers. The VLIPS has advantages such as high-speed communication, lower deployment cost using existing lighting infrastructure and being less vulnerable to interference than conventional radio frequency-based technology [5]. In brief, these advantages made the VLIPS a promising technology to be adopted for INSs.

The environment factors such as ambient light has a significant impact on how well the VLIPS performs. For instance, sunlight is one of the inference as its spectrum contains 48% of visible light [6]. As a result, there will be some issues caused by the discrepancy between simulation performance and hardware prototype performance. Firstly, when the proposed system is implemented in hardware, the system performance may change for current studies that have merely used simulation findings for the proposed system. Furthermore, if the testing environment has been greatly modified for existing efforts that merely include hardware development, the findings may be different. Therefore, a crucial issue for VLIPS is the design of a VLIPS that aligns with both the outcomes of the simulation framework and the performance of the hardware prototype.

Despite the fact that various research studies on the VLIPS have been undertaken, many overlook the consistency between the simulation and hardware prototype outcomes. The majority of the works, in particular, are solely concerned with simulation or hardware prototypes. Similarly, even though there have been various efforts on both simulation and hardware, the findings obtained are inconsistent [7]. It should be noted that a simulation framework aligned with the hardware findings assists in accelerating early VLIPS development by allowing developers to precisely simulate system performance for various LED installation configurations. As a result, VLIPS early development becomes more cost-effective and efficient, and hence a wide adoption of VLIPS is plausible. The main objective of this research is to investigate the feasibility of a simulation approach to simulate the environmental impacts exhibited in received signal strength (RSS) based VLIPS aligned with a prototype for more effective deployment of VLIPS. The contributions of this research are as follows:

i. A received signal strength-based VLIPS design was proposed and a corresponding hardware prototype was developed.
ii. The effects of the environmental impacts (external optical source and blocked transmitter) on the VLIPS accuracy were determined.
iii. A simulation framework modelling the environmental impacts capable of reproducing the effects similar to the prototype outcome was developed.

2. Indoor Positioning Technologies

In this section, some of the latest works on indoor positioning systems (IPS) using different technologies and approaches are reviewed to identify and understand the strengths and weaknesses of the IPS of different types of technology. First of all, Hosseini *et al.,* [8] proposed a new approach based on fingerprinting (FP) to improve the Wi-Fi-based IPS in multi-floor buildings. The approach proposed groups FPs into three sub-schemes: access points' RSS, users' last estimated location, and map-constrained graph. The research findings showed a 6%, 47%, and 67% improvement in accuracy for each of the sub-schemes, as well as an execution time reduction of 1.5 - 10 times. Next, Gentner *et al.,* [9] evaluated the Wi-Fi round-trip-time (RTT) protocol's distance estimation and positioning performance using Google Pixel 3 and Google Wi-Fi APs. The evaluation's findings showed positioning errors of 97% below 1 m for a robot without person obstructions, 92% below 1 m for a robot with people moving around, and 70% below 1 m in the case of moving people. On the other hand, Cao *et al.,* [10] proposed an approach called line-of-sight (LOS) identification based on scenario recognition to assist the Wi-Fi RTT positioning to improve its accuracy. The research findings showed the proposed approach outperforms the least square algorithm, with a mean error of 0.826 m and root mean square error of 0.989 m.

For Bluetooth low energy (BLE) based IPS, Spachos and Plataniotis [11] used received signal strength indication (RSSI) and the Kalman filter (KF) to localize visitors in a museum. The transmitters were Gimbal Series 21 beacons, and the receiver was an LG Nexus 5 with Bluetooth 4.0. The experimental findings for distance estimation error are as follows: 95% less than 3m in the laboratory and 95% less than 3.5m in the corridor, both without KF. It is less than 2m for the laboratory and less than 2.5m for the corridor when KF is utilised. The impacts of transmitter topology were also investigated in this paper. In addition, K. Huang, He, and Du [12] proposed a hybrid method to mitigate the issue of RSSI variation and long-time intervals under the dense Bluetooth environment. The method included the trilateration algorithm, dead reckoning (DR) and KF. The experimental results indicated that the root-mean-square error (RMSE) of 0.757m was achieved.

For the RFID-based, Cheng *et al.,* [13] proposed a system with the combination of deep learning with RFID. The system used the tags information such as RSSI, phase, and timestamp to train the model. The experimental results indicate that the system's average positioning error is 10.02 cm. In the other work, an improved KNN-based UHF RFID indoor positioning algorithm was presented by Shi *et al.,* [14]. The work also derived an RSSI estimation model for a directional radiation scenario with multipath propagation from the floor considered. The simulation results showed that the system achieved an estimation error of 90% less than 0.6 m.

Other than the Wi-Fi-based, BLE-based and RFID-based IPS, the latest IPS works for the other radio frequency (RF) based technology such as ZigBee and ultra-wideband (UWB) were reviewed as well. Dong, Xu, and Zhuang [15] studied the RSSI-based ZigBee sensor network ranging and positioning technology using the TI-CC2431 chip. It adopted an average filter model and a Gaussian filter model to improve the accuracy as well as the triangulation method for distance measurements. Ultimately, the experimental data were obtained and an RSSI ranging model parameters were estimated using MATLAB simulation. Guo *et al.,* [16] performed a similar work using the TI-CC2530 chip and proposed the particle swarm optimization (PSO) method to improve the model parameters estimation. Besides, the authors used the k-nearest neighbour (KNN) algorithm for positioning. The experimental results indicated the mean errors of 3.54 m and 3.13 m for k=3 and k=4, respectively. On the other hand, Ni *et al.,* [17] proposed a three-dimensional TOA algorithm for UWB and a combination of least square linear estimation with KF for error reduction due to interference in transmission. The MATLAB simulation results showed that the system achieved a maximum error of 10 cm and a minimum error of 5 cm. In addition, Santoro *et al.,* [18] presented an experimental validation on their proposed model based on a novel ranging technique called downtime TDOA (DTDOA). The experimental results showed a maximum of 30 cm of uncertainty for the proposed system, which validated their proposed model. Therefore, it was shown that the RF-based IPS rarely can achieve a centimetre level of accuracy. Furthermore, the Wi-Fi-based IPS also faces challenges such as a limited number of antennas on Wi-Fi devices, limited channel bandwidth, and highly accurate time synchronization difficulty [19].

In addition, there are some works for non-RF-based IPS that were reviewed such as ultrasonic-based and visible light (VL)-based. For example, Carotenuto *et al.,* [20] presented a self-synchronising indoor positioning technique to overcome the synchronisation requirement in ultrasonic systems using time-of-arrival (TOA) and time-difference-of-arrival (TDOA). The work performed both simulation and experiments for the proposed technique. Ultimately, the results showed that an absolute positioning error of less than 5 cm for an office room under 8 Hz positioning rate was achieved and the simulation and experimental results are in good agreement. Although both simulation results and experimental results have been presented in this study and agreed well, ultrasonic technology is susceptible to temperature and humidity, as well as having a limited range for positioning [21].

Then, Lin *et al.,* [22] proposed a VL-based IPS by using a CMOS image sensor to receive the on-off keying modulated signal from the LEDs. The authors evaluated the system for both stationary and moving objects. The experimental results indicated an average positioning error of 3.93 cm for stationary objects, 1.49 cm for an object with a speed of 1 m/s speed, and 1.86 cm for an object moving at 2 m/s. Then, Plets *et al.,* [7] evaluated the VL- based positioning algorithm under typical square and star topologies. The authors carried out the simulation and experiments for both 2D and 3D trilateration algorithms. The results have shown that both the simulation result and experiment result do not agree where the positioning error in simulation for square is 95% below 7.4 cm while it is 95% below 28.7 cm in experiments using 2D trilateration. In addition, Liu *et al.,* [23] proposed a VL-based system using only one LED and one rotatable photodiode through a machine learning (ML)

approach. The proposed positioning process is implemented via two stages: area classification and positioning. The ML algorithms involved in this approach are random forest algorithm, extreme learning machine and the density-based spatial clustering of applications with noise (DBSCAN). The simulation results show that by using the proposed indoor VLP system with the rotatable PD and the hybrid algorithm, the maximum and averaged positioning errors of wall or corner zones drop from 137.96 cm and 15.63 cm to 38.34 cm and 1.43 cm, respectively. In addition, Zhang *et al.,* [24] proposed a method for VL-based IPS based on an embedded platform and optical frequency image recognition with artificial intelligence (AI). The approach analyses the position information from the coded optical frequency image received by a camera using a forward neural network, and then the positioning results are achieved.

After reviewing the latest works on the IPS across various technologies, the VL-based technology shows significant potential as a relatively cost-effective and high-accuracy indoor positioning system solution. Additionally, many works primarily focus on enhancing the existing positioning algorithm and technique such as implementing an ML or deep learning algorithm on the conventional methods. However, these studies often neglect to address the challenges that might arise in the system deployment stage. The challenges include a change in environment that can significantly impact the actual performance of the proposed system, potentially leading to proposed system localization failures in the worst-case scenario. Therefore, the development of a simulation framework that aligns with the system's actual hardware performance stands as a crucial solution to address this challenge.

3. Proposed Methodology

3.1 VLIPS Design Overview

In this section, the proposed design for the visible light indoor positioning system (VLIPS) is fully explained. The proposed VLIPS consists of two main blocks: a transmitter and a receiver. The transmitter consists of two major sections which are the signal modulation and the light-emitting diode (LED). On the other hand, the receiver is built up from multiple stages: photodiode, transimpedance amplifier (TIA), signals demodulation, distance estimation and coordinate estimation. The overview of the proposed VLIPS design is illustrated in Figure 2.

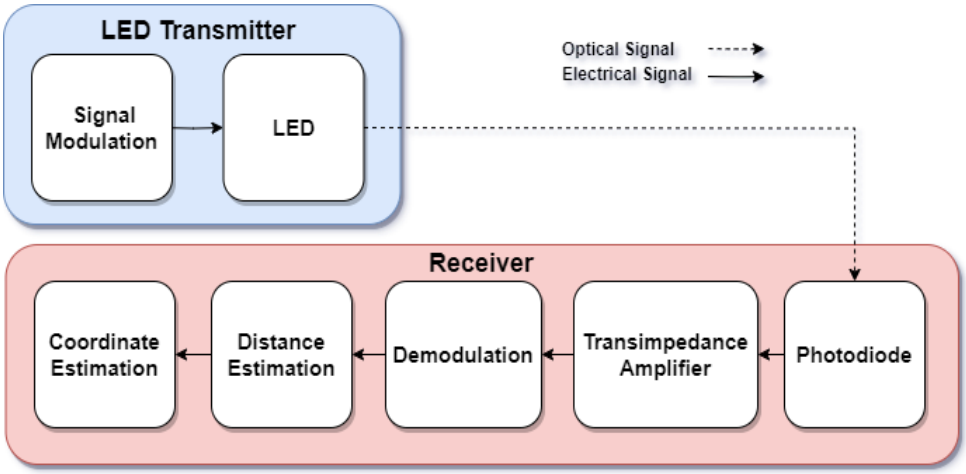

Fig. 2. Proposed VLIPS Design Overview

3.2 Signal Modulation and Demodulation

The modulation adopted in this system is based on the intensity modulation and direct detection (IM-DD) method. Basically, the LEDs in the proposed system will be switching on and off continuously according to a pulse width modulated (PWM) signal with distinct frequency, each frequency corresponds to each LED transmitter. On the other hand, the demodulation is performed through the fast Fourier transform (FFT) on the received signals to determine the signal amplitude for the unique frequencies assigned. The modulation method discussed results in a lower complexity of the system design which can help to speed up the VLIPS deployment stage.

3.3 Distance Estimation

For the proposed VLIPS to perform the localization, the distance between the photodiode receiver and the LED transmitters is required. Thus, the received signal strength (RSS) method was adopted for distance estimation purposes in the proposed VLIPS. The RSS method determines the distance based on the optical signal strength over distances characteristic of the LED. Theoretically, the characteristic mentioned can be determined through the Lambertian line-of-sight (LOS) channel DC gain equation as shown in Eq. (1) [25].

$$G_{LOS} = \frac{(m+1)A}{2\pi d^2}\cos^m(\phi)\cos^M(\psi) \tag{1}$$

Where G_{LOS} is Lambertian LOS channel DC gain, A is the photodiode effective area, ϕ is the LED transmitter angle to its normal, ψ is the receiver angle to its normal, d is the distance between an LED and the receiver, m and M are the Lambertian mode number that describes the LED transmitter and receiver's directionality, respectively. The values of m and M are determined through Eq. (2) and Eq. (3), respectively.

$$m = \frac{-ln2}{ln(cos(\phi))} \tag{2}$$

$$M = \frac{-ln2}{ln(cos(\psi))} \tag{3}$$

3.4 Localization Algorithm

The localization algorithm is the most essential part of the indoor positioning system to perform the localization of the target object effectively. For the proposed VLIPS, the trilateration algorithm is used to determine the receiver coordinate based on the distance of the photodiode receiver away from each LED transmitter determined through the RSS method discussed previously. Basically, the relationship between the distance determined with the photodiode receiver is related by the system of linear equations shown in Eq. (4) to Eq. (7).

$$(x_e - x_1)^2 + (y_e - y_1)^2 + (z_e - z_1)^2 = {d_{c_1}}^2 \tag{4}$$

$$(x_e - x_2)^2 + (y_e - y_2)^2 + (z_e - z_2)^2 = {d_{c_2}}^2 \tag{5}$$

$$(x_e - x_3)^2 + (y_e - y_3)^2 + (z_e - z_3)^2 = {d_{c_3}}^2 \tag{6}$$

$$(x_e - x_4)^2 + (y_e - y_4)^2 + (z_e - z_4)^2 = {d_{c_4}}^2 \quad (7)$$

Then, by solving the system of linear equations mentioned with the linear least square method, the receiver coordinate can be estimated as the matrix X shown in Eq. (8) [26].

$$X = \begin{bmatrix} x_e \\ y_e \end{bmatrix} = (A^T A)^{-1} A^T B \quad (8)$$

Where matrix A and matrix B are expressed as Eq. (9) and Eq. (10), respectively.

$$A = \begin{bmatrix} x_2 - x_1 & y_2 - y_1 \\ x_3 - x_1 & y_3 - y_1 \\ x_4 - x_1 & y_4 - y_1 \end{bmatrix} \quad (9)$$

$$B = \begin{bmatrix} \frac{({d_{c_1}}^2 - {d_{c_2}}^2 + {x_2}^2 + {y_2}^2 - {x_1}^2 - {y_1}^2)}{2} \\ \frac{({d_{c_1}}^2 - {d_{c_3}}^2 + {x_3}^2 + {y_3}^2 - {x_1}^2 - {y_1}^2)}{2} \\ \frac{({d_{c_1}}^2 - {d_{c_4}}^2 + {x_4}^2 + {y_4}^2 - {x_1}^2 - {y_1}^2)}{2} \end{bmatrix} \quad (10)$$

3.5 Hardware Implementation

In this section, the hardware implementation of the proposed VLIPS is discussed. To demonstrate the proposed VLIPS's hardware versatility and enhance the complexity of the hardware implementation from our prior work in [27], a different microcontroller was used in this paper with reduced hardware components compared to our prior work. For instance, the hardware implementation of the transmitter is realized with the ESP32 microcontroller, FQP50N06 MOSFET, and COB LED (BXRC-50C2000-C-24). For the signal modulation, the PWM signals will be generated from an ESP32 microcontroller and then turned on the FQP50N06L MOSFET. Eventually, the LED will be switching on and off with identical signal characteristics as the PWM signal generated by the ESP32. The schematic diagram of the transmitter hardware implementation is illustrated in Figure 3.

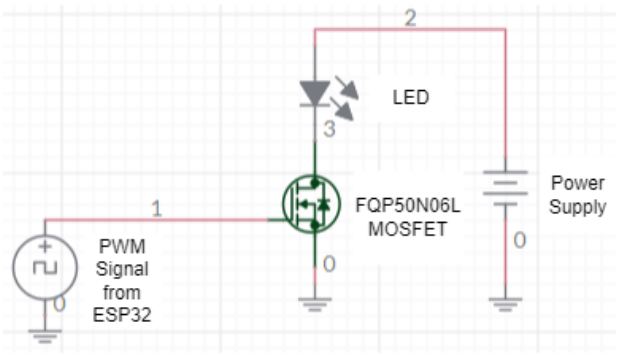

Fig. 3. Transmitter Circuit Schematic Diagram

Ultimately, 4 LED transmitters were constructed similarly for the proposed VLIPS as illustrated in Figure 4.

Fig. 4. LED Transmitters Prototype

Then, for the receiver section, the hardware implementation is realized with the use of an OPT101 photodiode with an on-chip TIA and another ESP32 microcontroller. Basically, the photodiode serves the role of receiving and converting the transmitted optical signals from the LED transmitters. Then, the ESP32 microcontroller was programmed to perform the FFT on the photodiode's output signal. Next, with the demodulated signal, the received signal strength of the unique frequency was determined. Then, Eq. (1) for the RSS distance estimation method, Eq. (8) to Eq. (10) for the trilateration localization algorithm were coded together with the LED transmitter's coordinates in the ESP32 program to localize the receiver position.

3.6 Simulation Framework Development

In this research, a simulation framework for the proposed VLIPS was developed using the Simulink where the complete development steps were presented in our works in [28]. The simulation framework is comprised of three parts: LED transmitters, the channel and the receiver as illustrated in Figure 5, Figure 6, and Figure 7, respectively. In transmitters, as shown in Figure 5, there is a signal modulation process to modulate the LED optical signals.

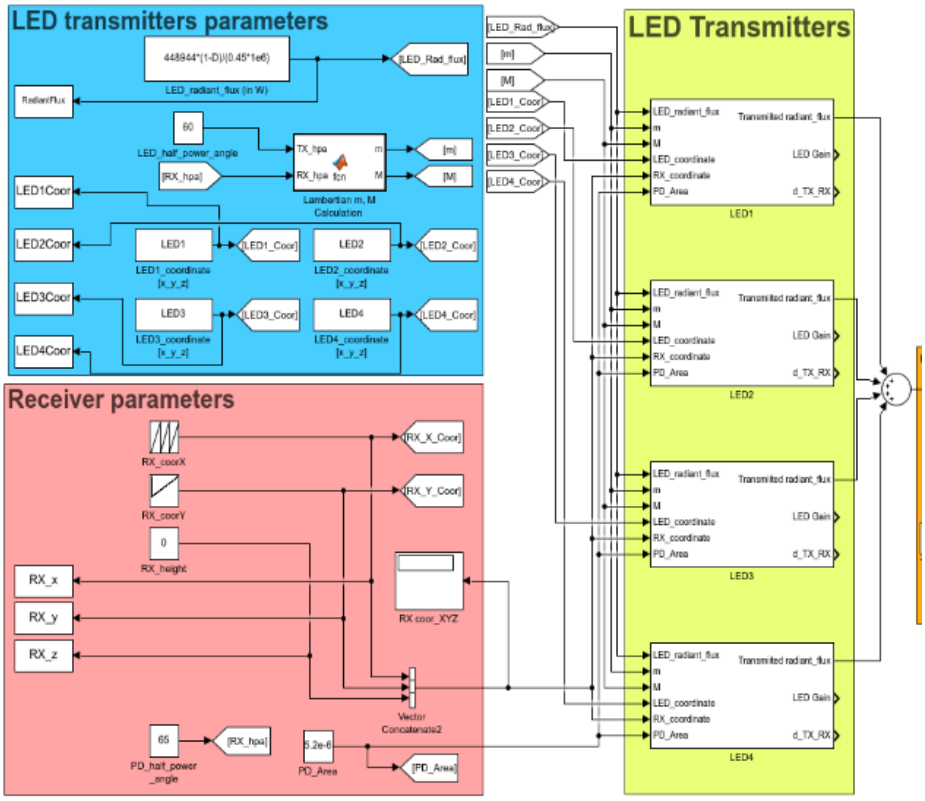

Fig. 5. Proposed VLIPS Simulation Framework – LED Transmitters

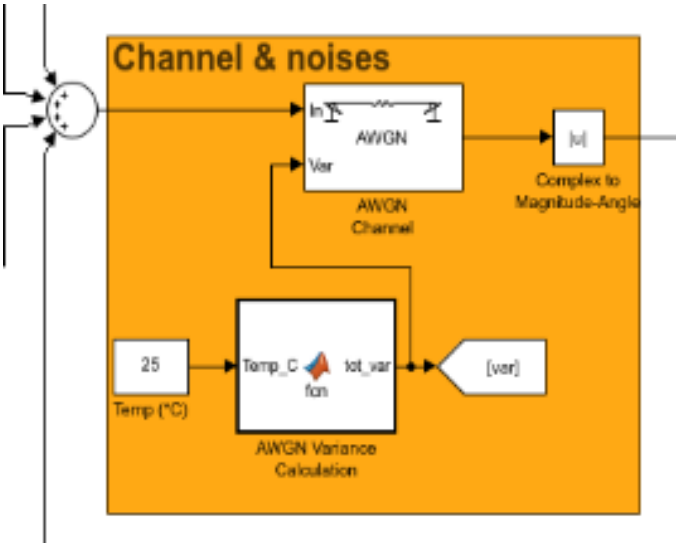

Fig. 6. Proposed VLIPS Simulation Framework – Channel

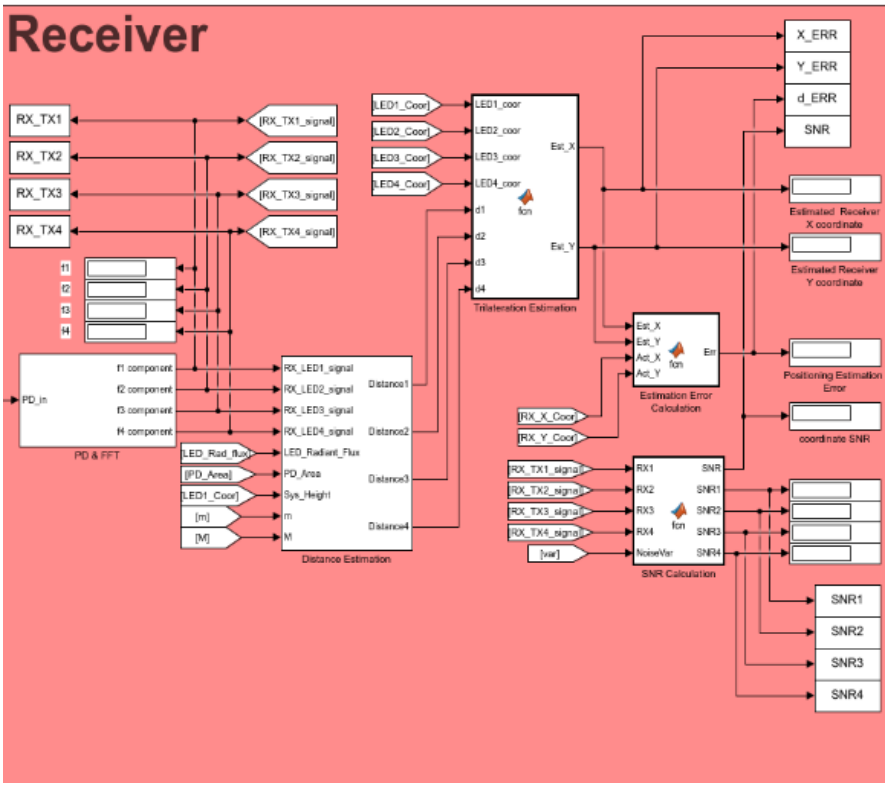

Fig. 7. Proposed VLIPS Simulation Framework – Receiver

In the channel, as shown in Figure 6, noise such as the shot noise, thermal noise and dark current noise was included. The noises are modelled as total noise variance, δ^2 of the additive white Gaussian noise (AWGN) channel, which is expressed as Eq. (11) [29].

$$\delta^2 = \delta_{ss}^2 + \delta_{js}^2 + \delta_{dc}^2 \tag{11}$$

where δ_{ss}^2 is the shot noise in the photodiode, δ_{js}^2 is the variance caused by thermal noise or Johnson noise in the photodiode and δ_{dc}^2 is the variance caused by the dark current of the photodiode, which is expressed as Eq. (12) to Eq. (14).

$$\delta_{ss}^2 = 2qR_I(P_r)B \tag{12}$$

$$\delta_{js}^2 = \frac{4KTB}{R_L} \tag{13}$$

$$\delta_{dc}^2 = 2qI_{dc}B \tag{14}$$

where q is the electron charge, R_I is the photodiode current responsivity, P_r is the radiant power received by the photodiode, B is the system bandwidth, K is the Boltzmann constant, T is the equivalent temperature in Kelvin, R_L is the load resistance and I_{dc} is the photodiode dark current.

Lastly, the receiver part as shown in Figure 7 consists of a photodiode to convert the received optical signals into electrical signals. Then, the fast Fourier transform (FFT) process is required to output the signals' amplitude in the frequency domain. The signals' amplitude values are then going through a received signal strength (RSS) computation process to determine the strength of the modulated signals. The values of strength are fed into the trilateration algorithm for distance

estimation between the receiver and transmitters. Ultimately, with all the distance between the receiver and each LED transmitter determined, the positioning error and SNR calculation can be computed at the final stage.

3.7 Testing Environments

In this section, the setup for prototype testing will be discussed thoroughly. Basically, the hardware prototype was carried out the testing in three environments: a room without influences, a room with an additional LED source, and a room with a transmitter blocked. The prototype parameters are listed in Table 1.

Table 1
Prototype System Parameters

Parameter	Value
LED Transmitters (TXs) Coordinate (in m): [LED1], [LED2], [LED3], [LED4]	[0, 0, 0.9], [0, 0.9, 0.9], [0.9, 0.9, 0.9], [0.9, 0, 0.9]
LED TXs Modulation Frequency: LED1, LED2, LED3, LED4	1.00 kHz, 1.25 kHz, 1.50 kHz, 1.75 kHz
LED TX Supply Voltage:	31V
Photodiode effective area:	5.2441 mm^2

For the testing, the system prototype was deployed in a setting such that the distance between each transmitter was 0.9 m. The LED transmitters were deployed at a height of 0.9 m as well. The setup mentioned resembles a room with a dimension of 0.9 m × 0.9 m × 0.9 m as shown in Figure 8.

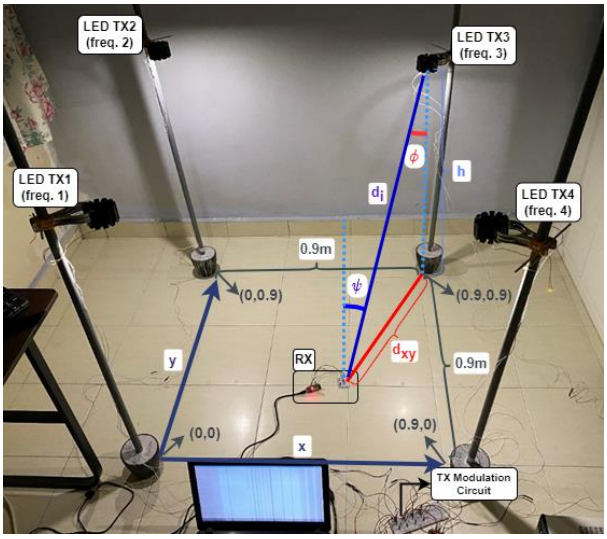

Fig. 8. Prototype Testing Setup

3.7.1 Room without influences

For the first test, the system prototype was deployed in a setting such that the influences from the surroundings were minimized. The objective of this testing is to obtain the ideal system performance data where the impacts from the environment are negligible to the received signal strength. These performance data will be used as the reference data for the comparison with the performance data in the following two testing environments. The prototype setup of this experiment is shown in Figure 9.

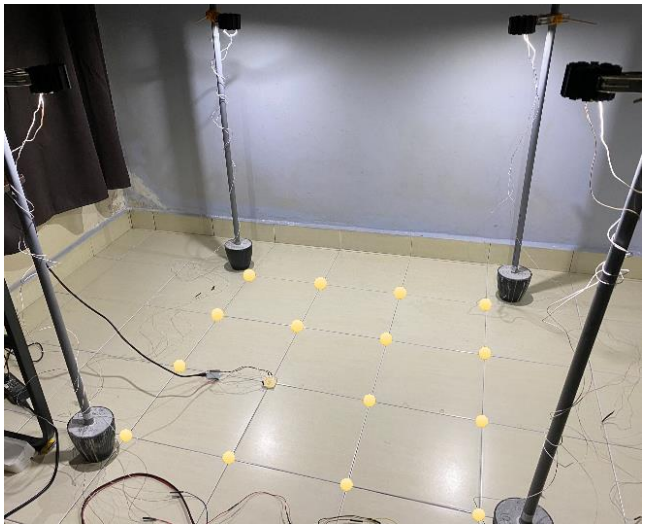

Fig. 9. Prototype Setup in a Room without Influences

3.7.2 Room with additional LED source

In this setup, an additional LED which is the same model as the LED transmitter was introduced into the setup. The objective of this experiment is to replicate the condition where there are some extra LEDs only required for illumination purposes but not as an LED transmitter in the system. The effect of the additional unmodulated LED was studied in this experiment, and the impact on the system performance was examined by comparing this set of experiment data with the ideal system performance data obtained in the first experiment discussed in section 3.7.1. The testing environment setup is shown in Figure 10.

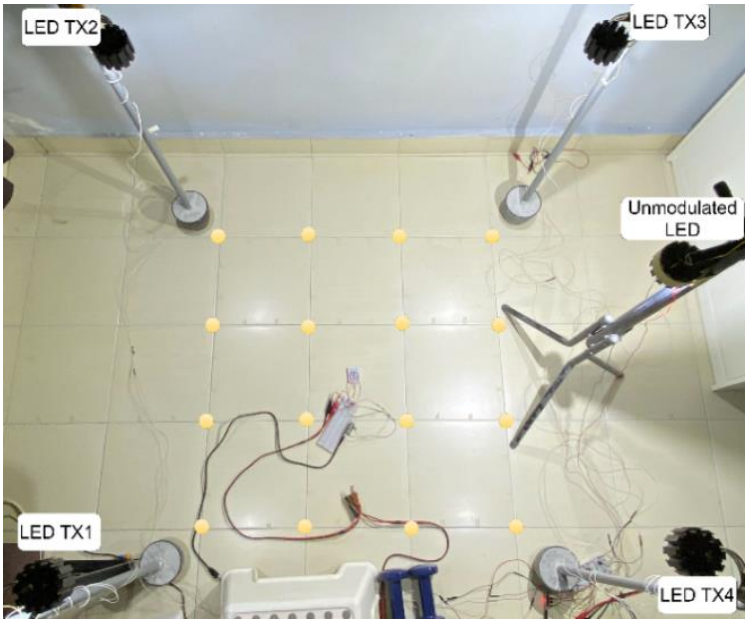

Fig. 10. Prototype Setup in a Room with Additional LED Source

3.7.3 Room with blocked transmitter

In this experiment, one of the LED transmitters (LED TX1) was completely blocked. The objective of this experiment is to replicate a condition where the LED transmitter was blocked by an obstacle

or when one of the LED transmitters failed to operate. In this experiment setup shown in Figure 11, LED transmitter 1 with the modulation frequency of 1 kHz was completely blocked. Therefore, the optical signal from the LED transmitter 1 is not possible to be received by the receiver. The data obtained in this experiment was compared with the ideal system performance data obtained in the first experiment discussed in section 3.7.1 to study the impact of blockage on the proposed system.

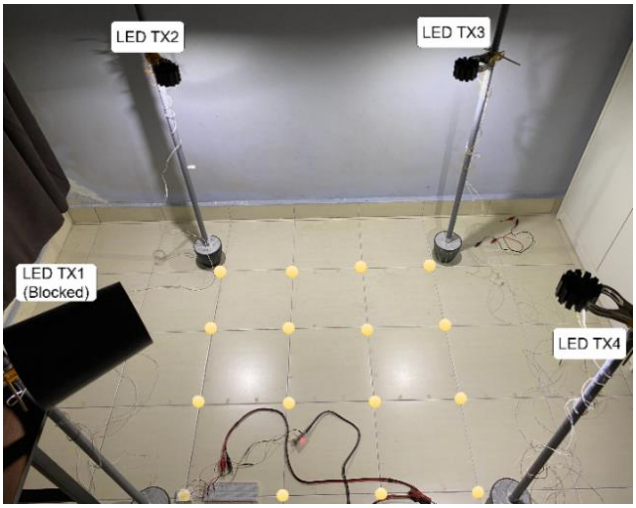

Fig. 11. Prototype Setup in a Room with Blocked LED Transmitter

4. Results and Discussion

4.1 Hardware Prototype Performance

The hardware prototype was tested in three different environments: a room without influences, a room with additional LED, and a room with a blocked transmitter (LED TX1). As such, the performance data such as the positioning error of the hardware prototype in three environments were obtained. As shown in Figure 12, the prototype positioning performance in three environments is shown as the comparison of the actual receiver coordinates and the estimated receiver coordinates.

Firstly, for the room without influences as shown in Figure 12(a), the difference between the estimated coordinates and actual coordinates is smaller as it is near the centre of the room, whereas the coordinates at the corner and boundary region have higher positioning errors. Therefore, the prototype positioning performance is better at the centre region when there are no influences from the environment and this will be used as a reference to be compared with the performance at the other two environments.

Next, for the room with an additional unmodulated LED source shown in Figure 12(b), the results showed that the positioning performance was degraded significantly. For instance, the estimated coordinates in this environment have having higher difference with the actual compared to experiment 1. Moreover, the prototype failed to perform the positioning with acceptable error at six coordinates, which are the coordinates near the additional LED at the coordinates of (0.9, 0.45, 0.9). This is because the extra optical signal strength from the additional LED was also accounted as the extra DC signal amplitude in the signal processing stage of the receiver. The high DC signal amplitude from this LED will cause two problems at two stages: photodiode and microcontroller analogue-to-digital conversion. The high DC amplitude signal multiplexed with the transmitter signals, caused the saturation to occur at the stages mentioned earlier. Ultimately, this distorted the transmitter signals and hence affected the positioning performance.

Lastly, for the room with LED transmitter 1 located at the coordinate of (0, 0, 0.9) blocked shown in Figure 12(c), the results obtained showed that the positioning performance dropped drastically at the coordinates near the blocked LED transmitter. However, for the coordinates that are nearer to the other three LED transmitters, the impact is relatively lower. This is due to a low received signal strength problem for all four transmitter signals at the blocked transmitter location, which caused the localization algorithm to perform precisely.

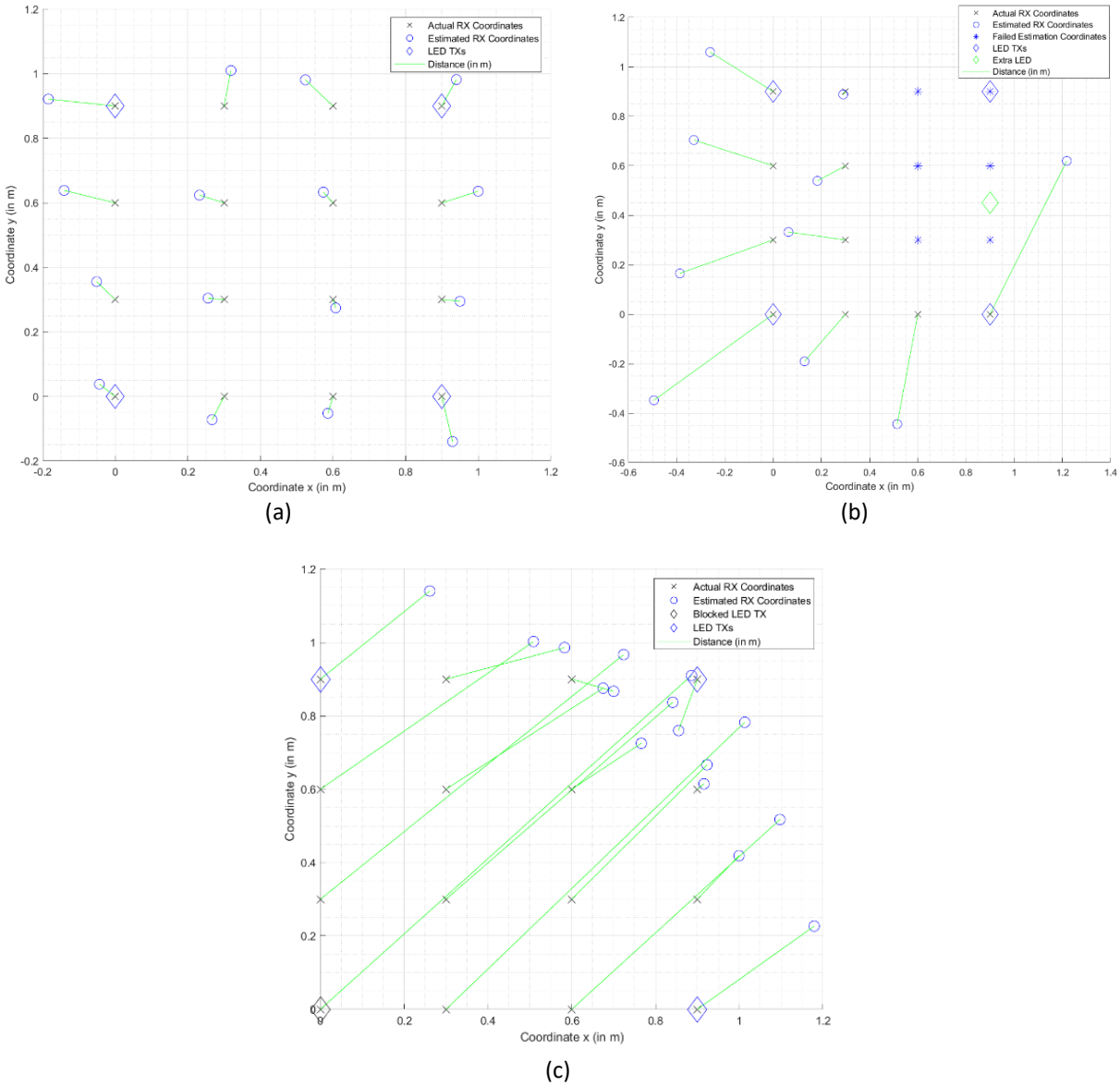

Fig. 12. Hardware Positioning Performance in Room (a) without Influences (b) with additional LED (c) with Blocked Transmitter

Subsequently, an empirical cumulative distribution function (ECDF) for the positioning error data obtained for three experiments was generated to analyse the impacts of the two environmental factors. Based on the ECDF shown in Figure 13, it was shown that the prototype in the room without influences achieved the positioning error within 8.36 cm for 50% of the time and within 20.33 cm for 90% of the time. Secondly, in the room with additional unmodulated LED, the prototype achieved positioning error within 35.41 cm for 50% of the time and within 87.03 cm for 90% of the time. Lastly, the prototype achieved positioning error within 1.1519 m for 50% of the time and within 1.2630 m

for 90% of the time in the condition of the blocked transmitter. Therefore, it showed that both additional lighting sources and blockage caused significant impacts on the proposed received signal strength (RSS) based visible light indoor positioning system (VLIPS), with the impact from blockage being the most significant to the system.

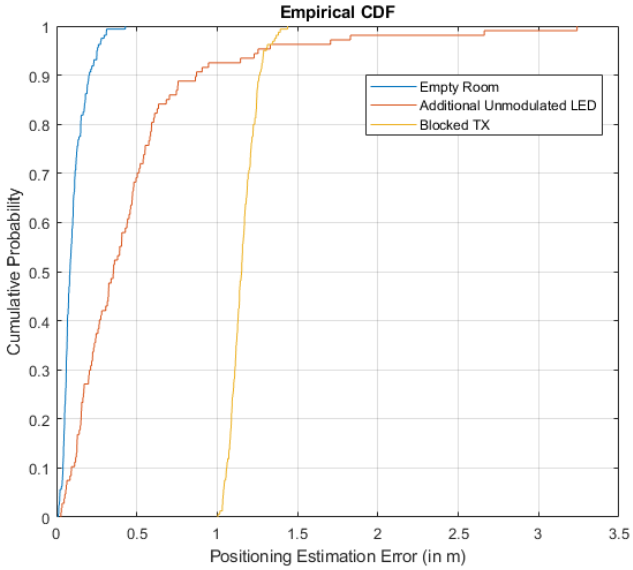

Fig. 13. Hardware Prototype Positioning Error ECDF Comparison

4.2 Simulation Performance

For the proposed VLIPS, the simulation for three environments tested by hardware prototype was carried out with the simulation framework developed. In the simulation, the samples were collected for 10000 coordinates in a room with the same setting as the hardware prototype setup. As such, the positioning error scatter plot of the simulation for three environments was obtained as shown in Figure 14.

Firstly, in the room without influences, the simulation obtained a trend similar to the hardware prototype result as shown in Figure 14(a), in which the positioning error is highest at the corner and boundary region and lower as it gets near the centre of the room. Next, for the results obtained for the room with the additional LED shown in Figure 14(b), the coordinates near the additional LED failed to perform positioning similar to the hardware prototype. However, in the simulation, the positioning error at the region near LED TX1 (0, 0, 0.9) and LED TX2 (0, 0.9, 0.9) are lower than the centre region instead of higher obtained in the hardware prototype. Lastly, the simulation results of the room with blocked transmitter LED TX1 shown in Figure 14(c), it was showed a similar trend as the hardware prototype result as well, where the error is higher for the coordinates near the blocked transmitter and lower as it near to the other three transmitters.

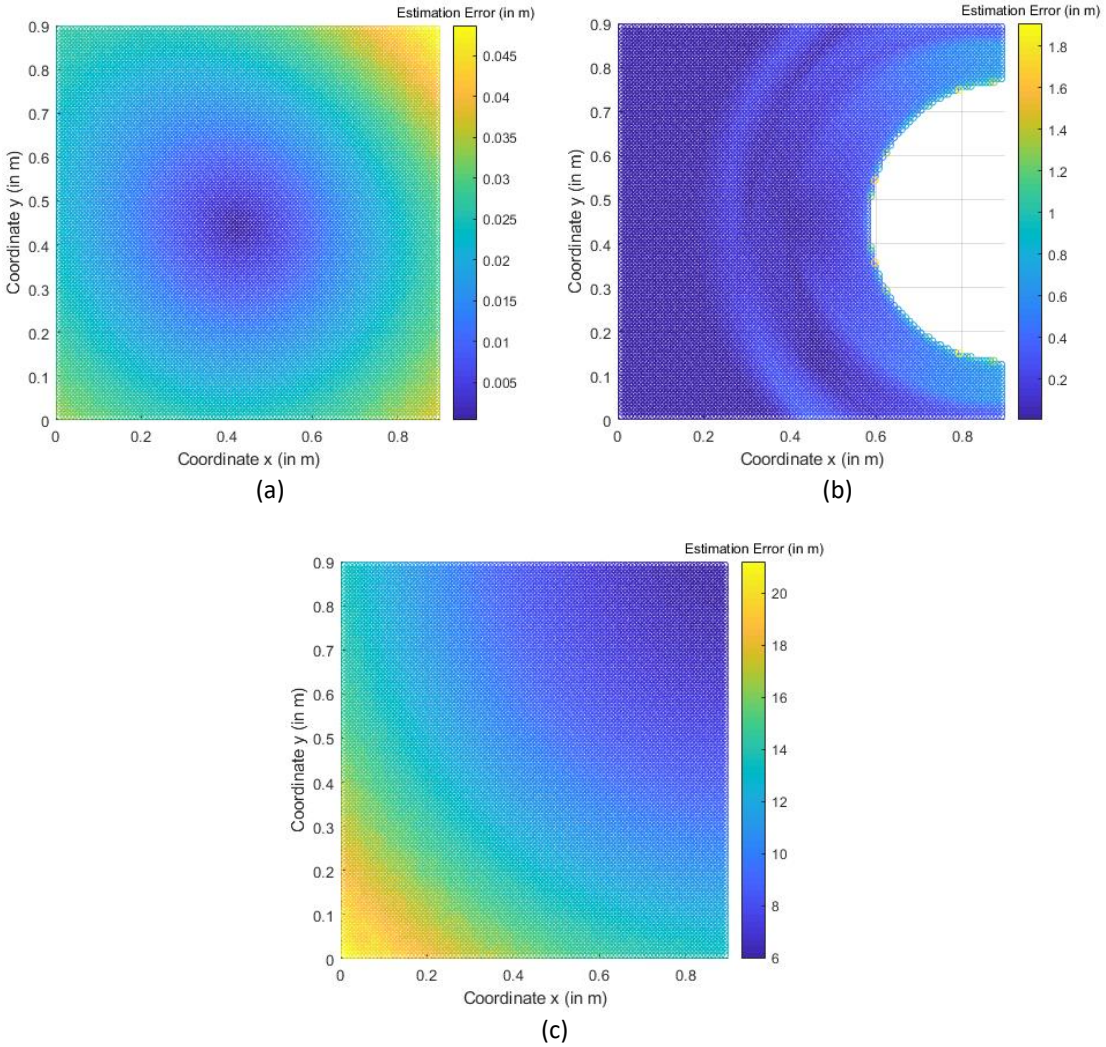

Fig. 14. Simulation Framework Positioning Performance in Room (a) without Influences (b) with additional LED (c) with Blocked Transmitter

Next, an ECDF of the positioning error data for the simulation results of three environments was generated to further analyse the difference between the simulation result and hardware. Based on the simulation results ECDF comparison shown in Figure 15, it was shown that the results in the room without influences achieved the positioning error within 2 cm for 50% of the time and within 2.96 cm for 90% of the time. Secondly, in the room with additional unmodulated LED, the prototype achieved positioning error within 8.9 cm for 50% of the time and within 39.61 cm for 90% of the time. Lastly, the prototype achieved positioning error within 11.1406 m for 50% of the time and within 15.6935 m for 90% of the time in the condition of the blocked transmitter.

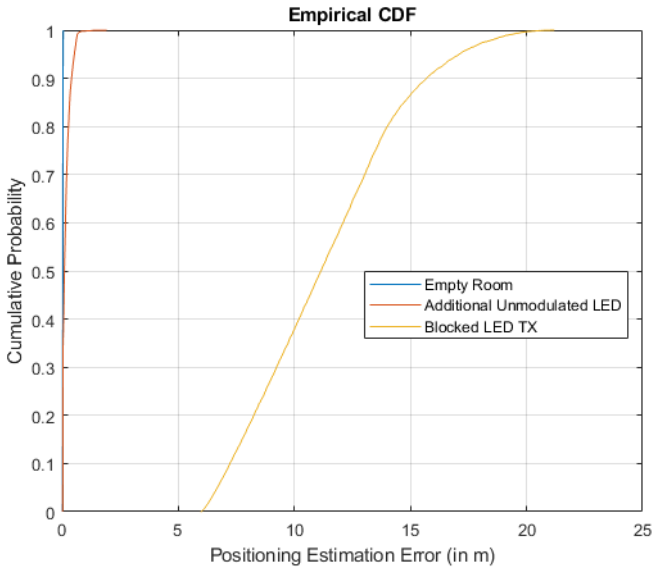

Fig. 15. Simulation Framework Positioning Error ECDF Comparison

4.3 Comparison between Hardware and Simulation

The simulation framework positioning error scatter plot results are overall similar to the hardware prototype obtained. Hence, to determine the difference between the results of the simulation framework and hardware prototype, a comparison of the metrics such as 50th percentile and 90th percentile from the results of each environment by both simulation framework and hardware was tabulated as Table 2. From the table, it was shown that the proposed simulation framework generated the results with lower positioning error compared to the hardware prototype for two environments: a room without influences and a room with additional LED. However, for the environment of a room with a blocked transmitter, the simulation result is higher than the hardware prototype. In summary, the simulation framework developed will generate results that are different from the hardware prototype with a minimum difference of 54.4870% and a maximum of 85.4402% on the 90th percentile metric for the room without influences and room without additional LED. On the other hand, the simulation framework will generate a result with a difference of 1142.5574%, which is greatly different from the hardware prototype for the room with a blocked transmitter environment.

Table 2
Results Comparison Between Simulation and Hardware Prototype

	Positioning Error [in m]					
	Room without Influences		Room with Additional LED		Room with Blocked Transmitter	
	50th Percentile	90th Percentile	50th Percentile	90th Percentile	50th Percentile	90th Percentile
Hardware Prototype (H) [m]	0.0836	0.2033	0.3541	0.8703	1.1519	1.2630
Simulation Framework (S) [m]	0.0200	0.0296	0.0890	0.3961	11.1406	15.6935
Percentage Error, $\frac{\lvert S-H\rvert}{H}\times 100$ [%]	76.0766	85.4402	74.8659	54.4870	867.1499	1142.5574

5. Conclusion

This paper proposed a simulation framework development for a visible light indoor positioning system (VLIPS) that aligns with hardware prototype positioning error results under three environments: a room without influences, a room with additional LED, and a room with blocked LED transmitter. For a room without any influences, the simulation framework achieved positioning errors of 2 cm and 2.96 cm for 50% of the time and 90% of the time, respectively. On the other hand, the hardware prototype obtained achieved positioning errors of 8.36 cm and 20.33 cm for 50% of the time and 90% of the time, respectively. The simulation framework developed was able to generate positioning error data with a similar trend as the hardware prototype obtained. However, there are differences in the exact values of the positioning error, with a maximum of 85.4402% and a minimum of 54.4870%. In addition, the simulation framework results for a room with a blocked transmitter have a huge difference from the hardware prototype. In conclusion, the proposed simulation framework can help the developer to identify the proposed VLIPS performance through the positioning error plot generated, but the differences between the simulation and hardware prototype result require improvement.

Our future work will focus on enhancing the accuracy of the simulation framework in non-line-of-sight conditions and incorporating additional environmental factors, such as multipath environments. In addition, the simulation framework developed can be used to generate datasets for training machine learning algorithms in saturation inference scenarios.

Acknowledgement
The study is partly sponsored under UTAR research fund.

References
[1] Technavio. "Indoor Positioning and Indoor Navigation Market by Application, Technology, and Geography - Forecast and Analysis 2023-2027." *Technavio*, (2023). https://www.technavio.com/report/indoor-positioning-and-indoor-navigation-market-industry-analysis

[2] Kunhoth, Jayakanth, AbdelGhani Karkar, Somaya Al-Maadeed, and Abdulla Al-Ali. "Indoor positioning and wayfinding systems: a survey." *Human-centric Computing and Information Sciences* 10 (2020): 1-41. https://doi.org/10.1186/s13673-020-00222-0

[3] Panda, Bibhuti, Harshvardhan Beria, and Chittaranjan Pradhan. "Deployment of Li-Fi in indoor positioning systems." *International Journal of Information Technology* 13 (2021): 123-130. https://doi.org/10.1007/s41870-020-00485-x

[4] Ee, Jonathan Yong Chung, Jin Yuan Chan, and Gan Lik Kang. "Carbon reduction analysis of Malaysian green port operation." *Progress in Energy and Environment* (2021): 1-7.

[5] Wen, DanQi. "Research progress of smart phone positioning and navigation sensors." In *Journal of Physics: Conference Series*, vol. 1930, no. 1, p. 012013. IOP Publishing, 2021. https://doi.org/10.1088/1742-6596/1930/1/012013

[6] Cheah, Kingsly Tian Chee, and Jing Yao Sum. "Synthesis and evaluation of Fe-doped zinc oxide photocatalyst for methylene blue and congo red removal." *Progress in Energy and Environment* (2022): 13-28. https://doi.org/10.37934/progee.22.1.1328

[7] Plets, David, Sander Bastiaens, Muhammad Ijaz, Yousef Almadani, Luc Martens, Willem Raes, Nobby Stevens, and Wout Joseph. "Three-dimensional visible light positioning: An experimental assessment of the importance of the LEDs' locations." In *2019 International Conference on Indoor Positioning and Indoor Navigation (IPIN)*, pp. 1-6. IEEE, 2019. https://doi.org/10.1109/IPIN.2019.8911763

[8] Hosseini, Komeil Shah, Mohammad Hadi Azaddel, Mohammad Amin Nourian, and Ahmad Akbari Azirani. "Improving Multi-floor WiFi-based Indoor positioning systems by Fingerprint grouping." In *2021 5th International Conference on Internet of Things and Applications (IoT)*, pp. 1-6. IEEE, 2021. https://doi.org/10.1109/IoT52625.2021.9469602

[9] Gentner, Christian, Markus Ulmschneider, Isabel Kuehner, and Armin Dammann. "WiFi-RTT indoor positioning." In *2020 IEEE/ION Position, Location and Navigation Symposium (PLANS)*, pp. 1029-1035. IEEE, 2020. https://doi.org/10.1109/PLANS46316.2020.9110232

[10] Cao, Hongji, Yunjia Wang, Jingxue Bi, Shenglei Xu, Minghao Si, and Hongxia Qi. "Indoor positioning method using WiFi RTT based on LOS identification and range calibration." *ISPRS International Journal of Geo-Information* 9, no. 11 (2020): 627. https://doi.org/10.3390/ijgi9110627

[11] Spachos, Petros, and Konstantinos N. Plataniotis. "BLE beacons for indoor positioning at an interactive IoT-based smart museum." *IEEE Systems Journal* 14, no. 3 (2020): 3483-3493. https://doi.org/10.1109/JSYST.2020.2969088

[12] Huang, Ke, Ke He, and Xuecheng Du. "A hybrid method to improve the BLE-based indoor positioning in a dense bluetooth environment." *Sensors* 19, no. 2 (2019): 424. https://doi.org/10.3390/s19020424

[13] Cheng, Shuyan, Shujun Wang, Wenbai Guan, He Xu, and Peng Li. "3DLRA: An RFID 3D indoor localization method based on deep learning." *Sensors* 20, no. 9 (2020): 2731. https://doi.org/10.3390/s20092731

[14] Shi, Weiguang, Jiangxia Du, Xiaowei Cao, Yang Yu, Yu Cao, Shuxia Yan, and Chunya Ni. "IKULDAS: An Improved k NN-Based UHF RFID Indoor Localization Algorithm for Directional Radiation Scenario." *Sensors* 19, no. 4 (2019): 968. https://doi.org/10.3390/s19040968

[15] Dong, Zhou Yang, Wei Ming Xu, and Hao Zhuang. "Research on ZigBee indoor technology positioning based on RSSI." *Procedia Computer Science* 154 (2019): 424-429. https://doi.org/10.1016/j.procs.2019.06.060

[16] Guo, Hang, Huixia Li, Jian Xiong, and Min Yu. "Indoor positioning system based on particle swarm optimization algorithm." *Measurement* 134 (2019): 908-913. https://doi.org/10.1016/j.measurement.2018.12.038

[17] Ni, Dongchen, Octavian Adrian Postolache, Chao Mi, Meisu Zhong, and Yongshuang Wang. "UWB indoor positioning application based on Kalman filter and 3-D TOA localization algorithm." In *2019 11th International Symposium on Advanced Topics in Electrical Engineering (ATEE)*, pp. 1-6. IEEE, 2019. https://doi.org/10.1109/ATEE.2019.8724907

[18] Santoro, Luca, Matteo Nardello, Davide Brunelli, and Daniele Fontanelli. "UWB-based indoor positioning system with infinite scalability." *IEEE Transactions on Instrumentation and Measurement* (2023). https://doi.org/10.36227/techrxiv.23284814.v1

[19] Qiao, Shuang, Chenhong Cao, Haoquan Zhou, and Wei Gong. "The trip to WiFi indoor localization across a decade—A systematic review." In *2023 26th International Conference on Computer Supported Cooperative Work in Design (CSCWD)*, pp. 642-647. IEEE, 2023. https://doi.org/10.1109/CSCWD57460.2023.10152700

[20] Carotenuto, Riccardo, Massimo Merenda, Demetrio Iero, and Francesco G. Della Corte. "Mobile synchronization recovery for ultrasonic indoor positioning." *Sensors* 20, no. 3 (2020): 702. https://doi.org/10.3390/s20030702

[21] Huang, Jiahao, Steffen Junginger, Hui Liu, and Kerstin Thurow. "Indoor positioning systems of mobile robots: A review." *Robotics* 12, no. 2 (2023): 47. https://doi.org/10.3390/robotics12020047

[22] Lin, Puxi, Xubin Hu, Yukui Ruan, Huaping Li, Junjian Fang, Yongchun Zhong, Huadan Zheng, Junbin Fang, Zoe Lin Jiang, and Zhe Chen. "Real-time visible light positioning supporting fast moving speed." *Optics Express* 28, no. 10 (2020): 14503-14510. https://doi.org/10.1364/OE.390781

[23] Liu, Ren, Zhonghua Liang, Kuo Yang, and Wei Li. "Machine learning based visible light indoor positioning with single-LED and single rotatable photo detector." *IEEE Photonics Journal* 14, no. 3 (2022): 1-11. https://doi.org/10.1109/JPHOT.2022.3163415

[24] Zhang, Feifan, Wei Ke, Hongxin Ouyang, and Shi Qiu. "Indoor visible light localization method based on embedded artificial intelligence." *The International Archives of the Photogrammetry, Remote Sensing and Spatial Information Sciences* 46 (2022): 255-261. https://doi.org/10.5194/isprs-archives-XLVI-3-W1-2022-255-2022

[25] Sheikh, Saad Mehmood, Hafiz M. Asif, Kaamran Raahemifar, and Fadi Al-Turjman. "Time difference of arrival based indoor positioning system using visible light communication." *IEEE Access* 9 (2021): 52113-52124. https://doi.org/10.1109/ACCESS.2021.3069793

[26] Chaudhary, Neha, Othman Isam Younus, Luis Nero Alves, Zabih Ghassemlooy, Stanislav Zvanovec, and Hoa Le-Minh. "An indoor visible light positioning system using tilted leds with high accuracy." *Sensors* 21, no. 3 (2021): 920. https://doi.org/10.3390/s21030920

[27] Foong, Jun Kit, Yuen Chark See, and Oon Ee Ng. "Indoor Positioning System using Light Emitting Diode." In *2021 IEEE 9th Conference on Systems, Process and Control (ICSPC 2021)*, pp. 7-12. IEEE, 2021. https://doi.org/10.1109/ICSPC53359.2021.9689178

[28] Foong, Jun Kit, and Yuen Chark See. "Signal-to-Noise Ratio in Indoor Navigation System Using Light Emitting Diode." In *2021 IEEE 19th Student Conference on Research and Development (SCOReD)*, pp. 24-29. IEEE, 2021. https://doi.org/10.1109/SCOReD53546.2021.9652763

[29] Maheepala, Malith, Abbas Z. Kouzani, and Matthew A. Joordens. "Light-based indoor positioning systems: A review." *IEEE Sensors Journal* 20, no. 8 (2020): 3971-3995. https://doi.org/10.1109/JSEN.2020.2964380